

Article

Finite Element In-Depth Verification: Base Displacements of a Spherical Dome Loaded by Edge Forces and Moments

Vasiliki G. Terzi *  and Triantafyllos K. Makarios 

Institute of Structural Analysis and Dynamics of Structures, School of Civil Engineering, Aristotle University of Thessaloniki, 56124 Thessaloniki, Greece; makariostr@civil.auth.gr

* Correspondence: terziv@civil.auth.gr

Abstract: Nowadays, engineers possess a wealth of numerical packages in order to design civil engineering structures. The finite element method offers a variety of sophisticated element types, nonlinear materials, and solution algorithms, which enable engineers to confront complicated design problems. However, one of the difficult tasks is the verification of the produced numerical results. The present paper deals with the in-depth verification of a basic problem, referring to the axisymmetric loading by edge forces/moments of a spherical dome, truncated at various roll-down angles, φ_0 . Two formulations of analytical solutions are derived by the bibliography; their results are compared with those produced by the implementation of the finite element method. Modelling details, such as the finite element type, orientation of joints, application of loading, boundary conditions, and results' interpretation, are presented thoroughly. Four different ratios of the radius of curvature, r and shell's thickness, and t are examined in order to investigate the compatibility between the implementation of the finite element method to the "first-order" shell theory. The discussion refers to the differences not only between the numerical and analytical results, but also between the two analytical approaches. Furthermore, it emphasizes the necessity of contacting even linear elastic preliminary verification numerical tests as a basis for the construction of more elaborated and sophisticated models.

Keywords: finite element method; thin shell; spherical dome; verification; modelling assumptions



Citation: Terzi, V.G.; Makarios, T.K. Finite Element In-Depth Verification: Base Displacements of a Spherical Dome Loaded by Edge Forces and Moments. *Modelling* **2024**, *5*, 37–54. <https://doi.org/10.3390/modelling5010003>

Academic Editor: Josef Kiendl

Received: 24 November 2023

Revised: 12 December 2023

Accepted: 19 December 2023

Published: 21 December 2023



Copyright: © 2023 by the authors. Licensee MDPI, Basel, Switzerland. This article is an open access article distributed under the terms and conditions of the Creative Commons Attribution (CC BY) license (<https://creativecommons.org/licenses/by/4.0/>).

1. Introduction

Nowadays, designers have the ability to implement various numerical methods in order to study an engineering problem. Sophisticated numerical models are produced by utilizing elaborated finite element types, laws of materials, analysis types, and loading and boundary conditions. However, the major difficult task is twofold and regards the process of the validation and verification of the numerical models, which acquires a particular significance [1]. In particular, the validation is related to the physics of the problem or otherwise, namely the correctness of the mathematical equations constructed for modeling certain mechanical phenomena. Furthermore, the verification is related to the correctness of the solution of the assumed approximation [2] or otherwise, namely the level of confidence that an approximate result corresponds to a given tolerance range of the exact solution of the mathematical model [3]. The aforementioned processes can be fulfilled by a comparison of the numerical results to laboratory/in situ experimental or analytical results [4,5].

The construction of shells, such as roofs of industrial buildings, pressure vessels, nuclear reactors, sports centers, and auditoriums, has been expanded in recent years, since they combine practical, functional, cost-effective, and aesthetic needs [6–8]. Among shells' structures, rotationally symmetric domes are frequently designed not only due to their small mass and high stiffness, but also due to their attractive architectural forms [9]. One of the principal modeling aspects that the designer faces is the decision of performing a "thin"/"thick" shell or fully three-dimensional analysis.

The theory of thin-walled shells is based on fundamental assumptions, which allows the efficient analysis of shell structures to be conducted in the two-dimensional rather

in the three-dimensional space [10,11]. The “thin” or “first-order” plate/shell theory, which is also known as the “Kirchhoff-Love” theory [12–15], is founded on the following assumptions [16]: (i) normals to the shell mid-surface remain straight and normal after deformation; (ii) the transverse normal stress is negligible (Figure 1a). Additional simplifications refer also to the following assumptions: (i) the strains receive very small values compared with unity [17,18]; (ii) the shell thickness remains constant. On the other hand, the “thick” or “second-order” plate/shell theory, which is also known as the “Mindlin-Reissner” theory, takes transverse shear deformation into account; therefore, the normals to the shell mid-surface do not remain normal after deformation (Figure 1b) [19,20]. As a general comment, it could be stated that the “first-order” and “second-order” plate/shell theories are the analogies of Euler–Bernoulli [21] and Timoshenko–Ehrenfest [22,23] beam theories, respectively [24].

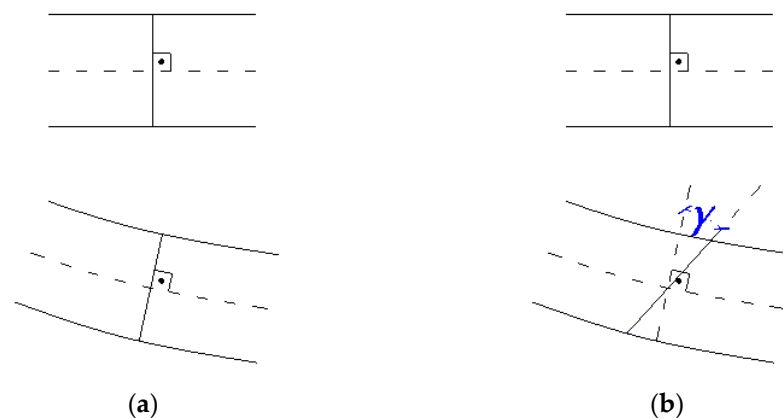


Figure 1. Deformation according to: (a) “thin”, $\gamma = 0 \rightarrow \tau = 0$ and (b) “thick” shell theory, $\gamma \neq 0 \rightarrow \tau \neq 0$.

The first question that arises is regarding the criteria under which the engineer will perform an analysis by the implementation of shell finite elements by applying the “first-order” or the “second-order” theory. Furthermore, an additional question that arises regards the criteria for the conduction of a full three-dimensional analysis by the implementation of solid finite elements. Both answers depend on the physics and geometric nature of the problem under study. However, Vlassov, in 1958 [25], proposed that the limit ratio between the radius of curvature, r , and the shell’s thickness, t , for the application of the “thin” shell theory, receives the value of $r/t = 30$. In 1959, Timoshenko and Woinowsky-Krieger proposed that if the shell’s thickness, t , is comparable to its radius of curvature, r , then the “second-order” theory should be applied or even a three-dimensional analysis should be conducted [26]. Additionally, in 1975, Flügge proposed that the “first-order” theory produces rigorous results in the case of the shell’s thickness, t , which is small [27] and is almost the same as the criterion of $r/t \gg 1$, proposed by Brush and Almroth [17]. In 1977, Heyman defined the limit ratio for the application of the “thin” shell theory as $r/t > 20$ [28]. Moreover, in 1983 and 1985, Calladine and Bushnell [15,16], respectively, defined the aforementioned limit ratio as $r/t = 10$.

The behavior of “thin” or “thick” shells under various loading conditions can be studied by a number of the available approaches: analytical [29–32]; a combination of analytical and numerical [33–36]; a combination of analytical, experimental, and numerical [37–40]; semi-analytical [41–43].

The development and evolution of numerical methods have limited the utilization of “thin” shell theory [3]. However, the comparison between analytical and numerical results remains a challenging task. The most characteristic case is the Girkmann problem [44], which refers to the behavior of a concrete spherical dome that is stiffened by a foot ring under a dead gravity load. The verification challenge was posed in 2008 by the International Association of Computational Mechanics (ICAM) to the finite element

community [45]. Different models and formulations were implemented during various verification processes [3,46–48].

The behavior of the shell is a combination of the membrane and bending theory. The membrane theory is valid only in shell regions that are sufficiently distant from supports; concentrated loads; geometrical discontinuities, such as shell thickness; slope; curvature [49–51]. In all of the aforementioned cases, membrane theory provides adequate solutions to each problem [52]. The present paper deals with a case of edge loading, which, even though it is a basic problem, has been poorly investigated. In particular, it refers to the in-depth verification of the implementation of the finite element method considering a basic problem of a spherical dome's behavior. The shell structure is loaded along its perimeter by edge horizontal forces and moments. The basic asset of the present paper is that two analytical formulations are derived by the bibliography, characterized as the first and second approximation, which refer to the determination of the base's translational and rotational displacements. Therefore, the necessary comparisons are performed between the results of the two analytical approaches. Fundamental aspects of the finite element modeling are investigated and discussed in detail, such as: the finite element type, mesh discretization, orientation of the joint coordinate system, the loading application, boundary conditions, and results' interpretation. In order to determine the limits of the application of the "thin" shell assumption, four different ratios r/t are taken into account. The numerical results are compared with the analytical ones. Both the convergence and differences are discussed in detail and are attributed to certain modeling aspects or theoretical assumptions.

2. Theoretical Background

Consider the spherical dome of radius, r , and thickness, t , which is truncated at a roll-down angle, φ_0 , increasing in clock-wise way (Figure 2). The circumference of the spherical cap is characterized by the radius, r_0 , and by the corresponding height, h_0 . The dome's material is considered as an isotropic linear elastic and is characterized by Young's modulus, E , and Poisson's ratio, ν .

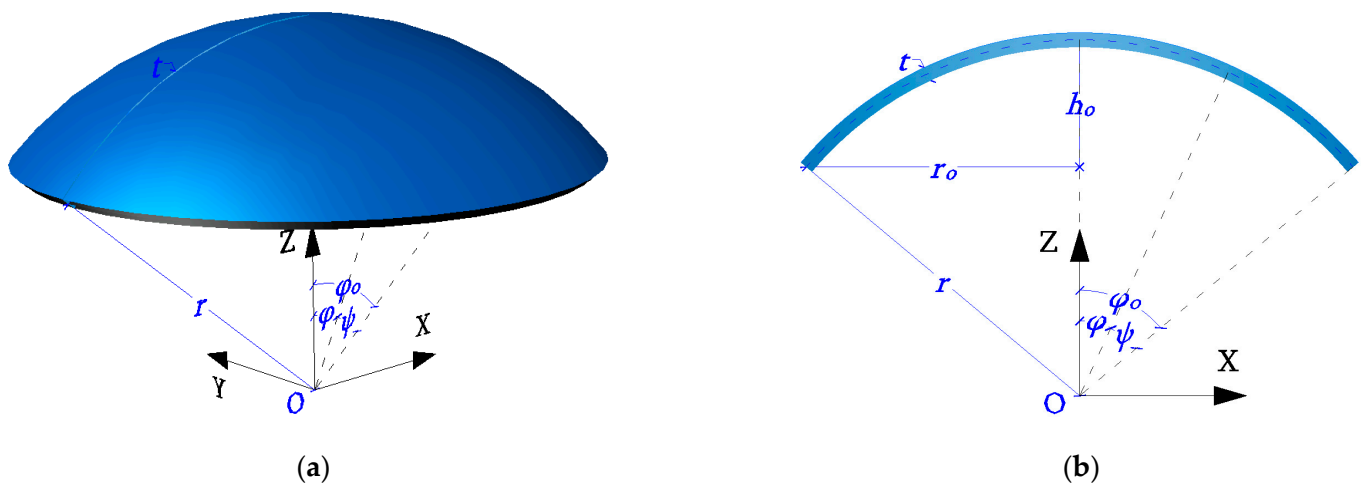


Figure 2. Truncated spherical dome representation: (a) 3d space and (b) 2d plane.

Figure 3 depicts the forces and moments which develop according to the membrane and bending theory of shells [26]. The forces N_φ , N_θ , and $N_{\varphi\theta} = N_{\theta\varphi}$ form the basis of the membrane theory. The moments M_φ , M_θ , and $M_{\varphi\theta} = M_{\theta\varphi}$, in combination with the transverse shear forces Q_φ and Q_θ , form the basis of the bending theory.

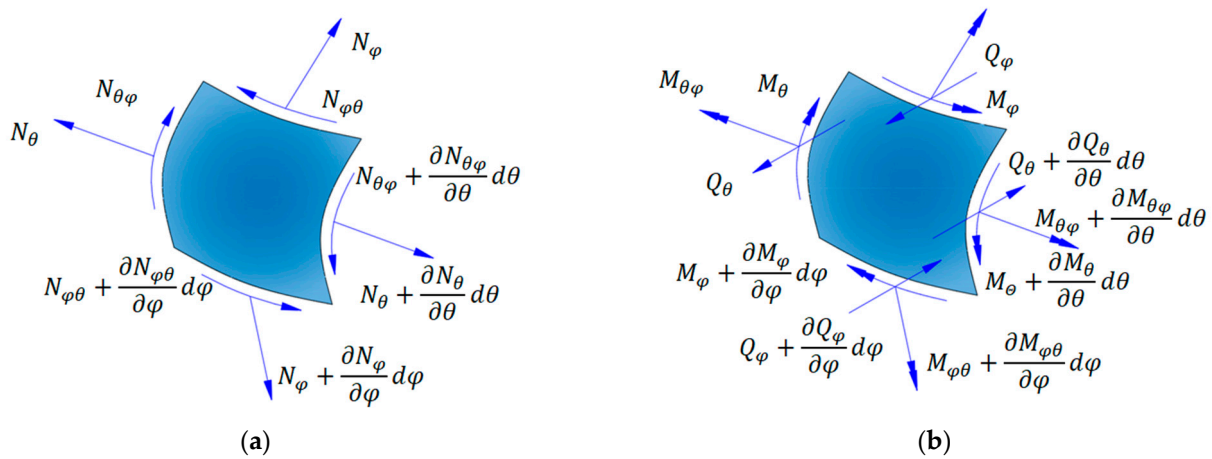


Figure 3. Forces and moments according to: (a) membrane theory; (b) bending theory.

The bending behavior of the spherical shell is described by the two approximated equations proposed by Geckeler J.W. [53].

$$\frac{d^2Q_\varphi}{d\varphi^2} + \cot\varphi \cdot \frac{dQ_\varphi}{d\varphi} + (\cot^2\varphi - \nu) \cdot Q_\varphi = E \cdot t \cdot V \tag{1a}$$

$$\frac{d^2V}{d\varphi^2} + \cot\varphi \cdot \frac{dV}{d\varphi} + (\cot^2\varphi + \nu) \cdot V = -\frac{r^2 \cdot Q_\varphi}{D} \tag{1b}$$

where V is the rotation of a tangent to a meridian; and $D = E \cdot t^3 / [12 \cdot (1 - \nu^2)]$. The shear force, Q_φ , receives the following form.

$$Q_\varphi = \frac{e^{\beta \cdot \varphi}}{\sqrt{\sin\varphi}} \cdot (C_1 \cdot \cos(\beta \cdot \varphi) + C_2 \cdot \sin(\beta \cdot \varphi)) \tag{2}$$

where

$$\beta^4 = \frac{1 - \nu^2}{4} \cdot \left(1 + \frac{12 \cdot r^2}{t^2}\right) \tag{3}$$

In the case of very thin shells and for large values of angle φ , both Q_φ and V are damped out rapidly as the distance from the edge increases. Furthermore, in the case of thin shells, according to Equation (3), β receives large values and the first derivative of Q_φ is large in comparison with Q_φ . Moreover, the second derivative of Q_φ is large in comparison with the first derivative of Q_φ . The aforementioned conclusions enable us to proceed with the approximation of neglecting the functions Q_φ and V, as well as their first derivatives in the left part of Equation (1). Therefore, Equation (1) receives the following form.

$$\frac{d^2Q_\varphi}{d\varphi^2} = E \cdot t \cdot V \tag{4a}$$

$$\frac{d^2V}{d\varphi^2} = -\frac{r^2 \cdot Q_\varphi}{D} \tag{4b}$$

Finally, the general solution of the shear force, Q_φ , is given by Equation (5).

$$Q_\varphi = C_1 \cdot e^{(\lambda \cdot \varphi)} \cdot \cos(\lambda \cdot \varphi) + C_2 \cdot e^{(\lambda \cdot \varphi)} \cdot \sin(\lambda \cdot \varphi) + C_3 \cdot e^{(-\lambda \cdot \varphi)} \cdot \cos(\lambda \cdot \varphi) + C_4 \cdot e^{(-\lambda \cdot \varphi)} \cdot \sin(\lambda \cdot \varphi) \tag{5}$$

where

$$\lambda^4 = 3 \cdot (1 - \nu^2) \cdot \left(\frac{r}{t}\right)^2 \tag{6}$$

Two cases of edge conditions along the dome’s perimeter are taken into account: (i) base force, H_o ; (ii) base moment, M_o (Figure 4). The edge force, H_o , causes the horizontal translation Δ_{H,H_o} and the rotation Δ_{φ,H_o} of the base. Furthermore, the edge moment, M_o , causes the horizontal translation Δ_{H,M_o} and the rotation Δ_{φ,M_o} of the base.

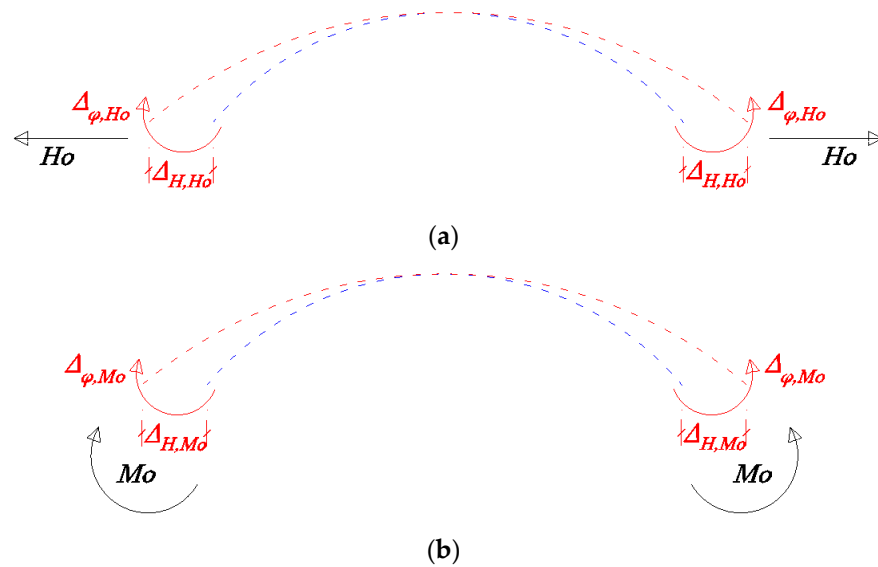


Figure 4. Edge conditions along the dome’s perimeter: (a) horizontal force and (b) moment [blue line: initial state; red line: deformed state].

In the case that the aforementioned two loading types are imposed on the shell’s edge and no hole exists at the top, Equation (5) can be simplified, as follows:

$$Q_\varphi = C_1 \cdot e^{(\lambda \cdot \varphi)} \cdot \cos(\lambda \cdot \varphi) + C_2 \cdot e^{(\lambda \cdot \varphi)} \cdot \sin(\lambda \cdot \varphi) \tag{7a}$$

$$Q_\varphi = C \cdot e^{(-\lambda \cdot \varphi)} \cdot \sin(\lambda \cdot \psi + \gamma) \tag{7b}$$

Therefore, for each loading type, two boundary conditions suffice in order to solve Equation (7a) in terms of C_1, C_2 or Equation (7b) in terms of C, γ . For the horizontal edge force, H_o , the boundary conditions are described by Equation (8), while for the edge moment, M_o , they are described by Equation (9). In particular, the horizontal force, H_o , which is applied at the edge, φ_o , produces only N_φ types of forces (Equation (8b)) and no edge moments, M_φ (Equation (8a)). Furthermore, the moment M_o , which is applied at the edge, φ_o , produces only M_φ moments (Equation (9a)) and no edge N_φ type of forces (Equation (9b)).

$$(M_\varphi)_{\varphi=\varphi_o} = 0 \tag{8a}$$

$$(N_\varphi)_{\varphi=\varphi_o} = -H_o \cdot \cos \varphi_o \tag{8b}$$

$$(M_\varphi)_{\varphi=\varphi_o} = M_o \tag{9a}$$

$$(N_\varphi)_{\varphi=\varphi_o} = 0 \tag{9b}$$

Timoshenko and Woinowsky–Krieger [26] provide, as a first approximation, Equation (10), in order to determine the dome’s base displacements under various values of the roll-down angle, φ_o . The first observation is that the rotation, due to the edge force, H_o (Equation (10b)), equals to the translation due to the edge moment, M_o (Equation (10c)), due to the reciprocity theorem, and under the assumption that $H_o = M_o$, since H_o and M_o , which are applied at the edge circumference of the dome, receive the same values expressed in kN/m or kNm/m, respectively.

The second observation refers to the rotation due to the edge moment, M_o (Equation (10d)). In particular, Δ_{φ, M_o} is independent of the roll-down angle, φ_o and corresponds to a fixed value.

$$\Delta_{H, H_o} = \frac{2 \cdot r \cdot \lambda \cdot \sin^2 \varphi_o}{E \cdot t} \cdot H_o \quad (10a)$$

$$\Delta_{\varphi, H_o} = \frac{2 \cdot \lambda^2 \cdot \sin \varphi_o}{E \cdot t} \cdot H_o \quad (10b)$$

$$\Delta_{H, M_o} = \frac{2 \cdot \lambda^2 \cdot \sin \varphi_o}{E \cdot t} \cdot M_o \quad (10c)$$

$$\Delta_{\varphi, M_o} = \frac{4 \cdot \lambda^3}{E \cdot r \cdot t} \cdot M_o \quad (10d)$$

Hetényi M., in 1937/1938, provided a closer approximation to the determination of the dome's base displacements, described by Equation (1) [54]. In particular, the following new variables were introduced.

$$Q_1 = Q_{\varphi} \cdot \sqrt{\sin \varphi} \quad (11a)$$

$$V_1 = V \cdot \sqrt{\sin \varphi} \quad (11b)$$

The quantities Q_{φ} and V are substituted in Equation (1); by applying the aforementioned procedure, the shear force is given by Equation (12).

$$Q_{\varphi} = C \cdot \frac{e^{(-\lambda \cdot \psi)}}{\sqrt{\sin(\varphi_o - \psi)}} \cdot \sin(\lambda \cdot \psi + \gamma) \quad (12)$$

The two unknowns, C, γ , are determined by the application of the boundary conditions that are described in Equations (7) and (8) and correspond to the two loading types. Finally, the equations of the displacements, according to Hetényi's approach, are described by the following:

$$k_1 = 1 - \frac{1 - 2 \cdot \nu}{2 \cdot \lambda} \cdot \cot \varphi_o \quad (13a)$$

$$k_2 = 1 - \frac{1 + 2 \cdot \nu}{2 \cdot \lambda} \cdot \cot \varphi_o \quad (13b)$$

$$\Delta_{H, H_o} = \frac{r \cdot \lambda \cdot \sin^2 \varphi_o}{E \cdot t} \cdot \left(k_2 + \frac{1}{k_1} \right) \cdot H_o \quad (13c)$$

$$\Delta_{\varphi, H_o} = \frac{2 \cdot \lambda^2 \cdot \sin \varphi_o}{E \cdot t \cdot k_1} \cdot H_o \quad (13d)$$

$$\Delta_{H, M_o} = \frac{2 \cdot \lambda^2 \cdot \sin \varphi_o}{E \cdot t \cdot k_1} \cdot M_o \quad (13e)$$

$$\Delta_{\varphi, M_o} = \frac{4 \cdot \lambda^3}{E \cdot r \cdot t \cdot k_1} \cdot M_o \quad (13f)$$

The comparison between Equations (10) and (13) leads to the conclusion that according to the second analytical approach, the rotation due to the edge moment, M_o (Equation (13f)), depends on the roll-down angle, φ_o , through the value of the k_1 parameter (Equation (13a)).

3. Finite Element Approach

Consider a spherical dome of the radius, $r = 25$ m, which is subjected to the edge force, $H_o = 1$ kN/m, and edge moment, $M_o = 1$ kNm/m, along its perimeter. In order to investigate the behavior of the "thin" shell finite element, four different cases of ratios r/t are taken into account: (i) 1000, (ii) 500, (iii) 100, and (iv) 30. The first three ones definitely

belong to the range of “thin” shells, while the fourth one belongs to the transitional area of the definition between “thin” and “thick” shells. The roll-down angle, φ_o , receives different values ranging from 5° to 90° by a step of 5° . The Young’s modulus of the concrete material equals to $E = 33$ GPa and the Poisson’s ratio equals to $\nu = 0.15$. All that is necessary for the calculations’ data are presented in Table 1.

Table 1. Data for calculations.

E [GPa]	ν [–]	r [m]	H_o [kN/m]	M_o [kNm/m]	r/t	φ_o [°]
33	0.15	25	1	1	30, 100, 500, 1000	5:5:90

3.1. Finite Element Modelling

The present section covers some of the basic modeling aspects, such as: (i) the finite element type; (ii) model discretization; (iii) orientation of the joint local coordinate system; (iv) loading definition; (v) boundary conditions; (vi) results’ interpretation. The finite element software applied for the analyses is SAP2000v.24 [55].

3.1.1. Finite Element Type

The homogeneous shell element, provided by SAP2000v.24, is implemented, since it combines independent membrane and plate behavior. Once the element is warped (non-planar), these behaviors become coupled. The isoparametric formulation is used by the membrane behavior, which includes both translational in-plane stiffness components and a “drilling” rotational stiffness in the direction normal to the plane of the element [56,57]. Two-way, out-of-plane, plate rotational stiffness components and a translational stiffness component in the direction normal to the plane of the element are included in the plate-bending behavior. The thin-plate or otherwise stated as the Kirchhoff formulation, which neglects the transverse shearing deformation, is chosen in order to achieve the compatibility between the numerical and analytical results. All the in-plane displacements are quadratic and all the out-of-plane displacements are cubic.

Figure 5 depicts the forces and moments, which develop in a typical shell element of SAP2000v.24 (grey colored). Each shell element possesses a local coordinate system denoted by 123 axes. The dashed line in the middle of its thickness corresponds to the mid-surface. Forces F_{11} , F_{22} , and F_{12} correspond to the membrane theory, while forces V_{13} and V_{23} are the transverse shear forces that correspond to the bending theory. Furthermore, moments M_{11} , M_{22} , and M_{12} also correspond to the bending theory. Both forces and moments are expressed in kN/m and kNm/m, respectively.

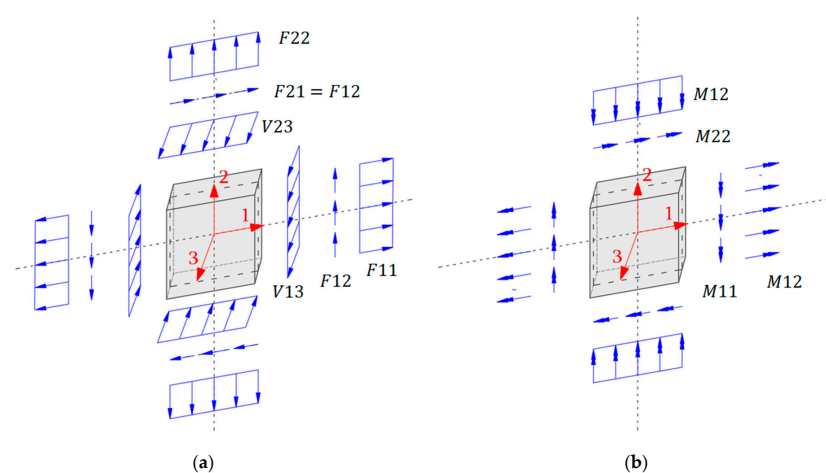


Figure 5. Shell finite element: (a) forces (membrane and bending theory); (b) moments (bending theory).

The analogy between the numerical and theoretical definitions of the forces' and moments' parameters is described as follows: $F11 = N_{\theta}$; $F12 = N_{\theta\varphi}$; $V13 = Q_{\theta}$; $F22 = N_{\varphi}$; $V23 = Q_{\varphi}$; $M11 = M_{\theta}$; $M12 = M_{\theta\varphi}$; and $M22 = M_{\varphi}$.

3.1.2. Model Discretization

The density and the number of finite elements in a model are of primary importance. The finite element mesh is produced automatically by the software, once certain values of the following geometry parameters are inserted: the radius of the spherical dome, r ; roll-down angle, φ_0 ; angular number of divisions; and number of divisions along height, h_0 . Special attention was given to the determination of the number of divisions. In particular, the discretization along the perimeter of the truncated spherical dome and along the height of the spherical cap must produce shell elements characterized by almost equal dimensions along the meridian and circumferential direction. The perimeter of the spherical cap equals to $L_0 = 2 \cdot \pi \cdot r_0$. The dimension of the base finite elements along the perimeter equals to $l_{f.e.,per.} = L_0 / n.o.d_{per.}$, where $n.o.d_{per.}$ is the number of divisions along the perimeter. The height of the spherical cap equals to $h_0 = r - r_0 / \tan \varphi_0$. Therefore, the number of divisions along the height is determined by the ratio, $n.o.d_{height.} = h_0 / l_{f.e.,per.}$.

In order to investigate the discretization effects on the numerical results, two different schemes were formulated: (i) coarse and (ii) dense mesh. Specifically, in the case of the coarse mesh discretization, the perimeter of the spherical cap of radius, r_0 , is divided into sections corresponding to an angle of 2° , while in the case of the dense mesh discretization, the aforementioned angle receives a value of 1° . Both discretization schemes lead to a high concentration of strains and stresses at the top of the spherical dome due to the high number of meridians that pass through. However, taking into account that the loading is not applied at the top but at the edges of the truncated spherical dome, and that the target is the estimation of the base displacements, the discretization effects at the top of the dome are considered to be not only local but negligible as well. In the case that the loading passes through the top of the dome, such as gravitational loading, or is applied exactly at the aforementioned point, as a concentrated force/moment, then the engineer should seek a different discretization scheme that lacks a node at this geometrical point. Furthermore, in order to achieve the optimum stress distribution, the mesh should be characterized by symmetry. Figure 6 depicts the two mesh formulations, which correspond to a spherical dome of a roll-down angle, $\varphi_0 = 40^\circ$.

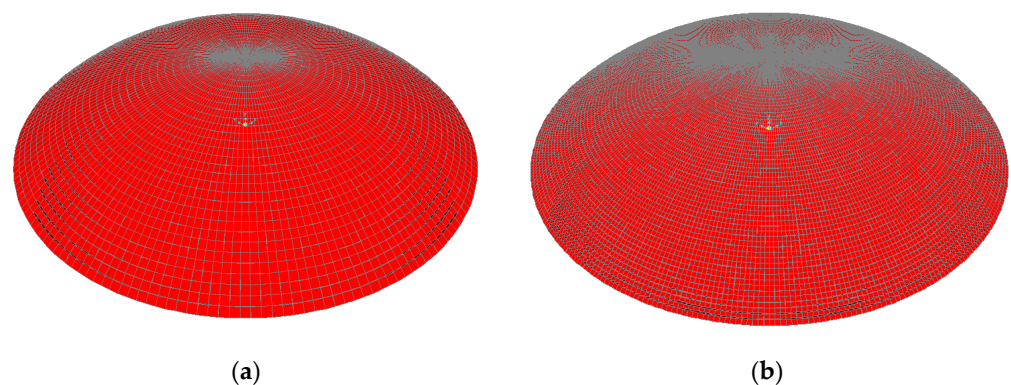


Figure 6. Model discretization: (a) coarse; (b) dense mesh.

3.1.3. Orientation of Joint Local Coordinate System

The joint local coordinate system is denoted as 123 in SAP2000 and coincides with the global coordinate system, XYZ. However, in order to achieve compatibility with the theoretical definitions, the local coordinate of the base joints is rotated around the: (i) Z and (ii) Y axis. The first rotation causes the local axis 1 to pass through the center of the spherical cap, while the second rotation causes the local axis 1 to pass through the center of the sphere. In this way, the local axis 3 is always tangential to the shell's mid-surface,

and the local axis 2 is perpendicular to the plane defined by local axes 1 and 3. Figure 7a depicts the final orientation of the joint local coordinate system in a typical cross-section, and Figure 7b depicts a typical rotated finite element of one of the created numerical models. The purple lines correspond to the bounding box of the finite element, while the grey plane corresponds to the shell's mid-surface. The red, white and cyan axes located at the mid-surface of the finite element correspond to local axes 1, 2, and 3, respectively. Axes 1 and 2 belong to the mid-plane, while axis 3 is perpendicular to it. Therefore, in correlation to Figure 5 (forces and moments), forces $F_{11} = N_{\theta}$ develop along the red axis, while forces $F_{22} = N_{\varphi}$ develop along the white axis. Furthermore, the red, white, and cyan axes located at the four nodes of the finite element correspond to local axes 1, 2, and 3, respectively.

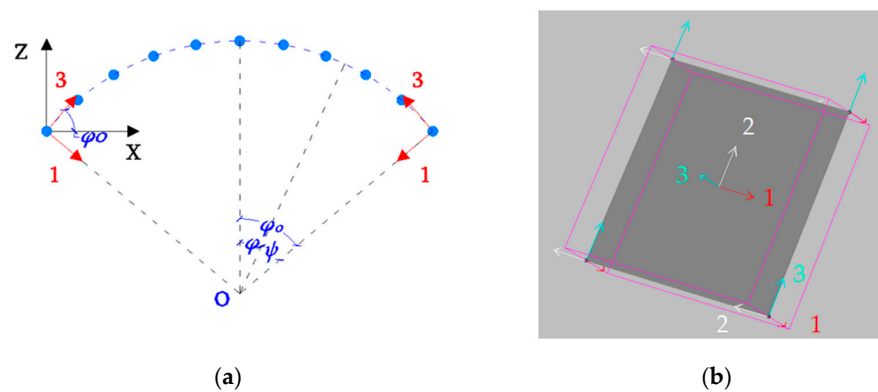


Figure 7. Local axes: (a) rotation of base joints (plane depiction); (b) final formulation of a typical finite element (3d depiction).

3.1.4. Loading Definition

According to the theory, the edge horizontal force receives the value of $H_0 = 1 \text{ kN/m}$, and the edge moment receives the value of $M_0 = 1 \text{ kNm/m}$. Therefore, in the finite element model, the horizontal force receives the value of $H_{0,fem} = H_0/n.o.n.$ and the moment receives the value of $M_{0,fem} = M_0/n.o.n.$, where n.o.n. corresponds to the number of nodes that belong to the perimeter of the spherical cap, according to each mesh discretization formulation. The loading is assigned as joint load (forces and moments). The value of the edge moment $M_{0,fem}$ is assigned to local axis 2 of the base joints. Furthermore, in the case of the horizontal load application, the edge force $H_{0,fem}$ is analyzed in two components along the joint local axes 1 and 3 by the application of Equation (14).

$$F_1 = -H_{0,fem} \cdot \sin\varphi_0 \tag{14a}$$

$$F_3 = -H_{0,fem} \cdot \cos\varphi_0 \tag{14b}$$

Figure 8 depicts the appropriate geometry for the definition of application of the horizontal edge load, $H_{0,fem}$.

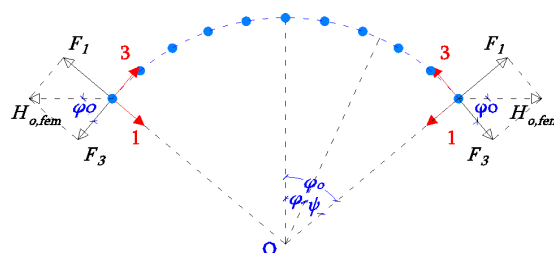


Figure 8. Application of horizontal edge load, $H_{0,fem}$.

3.1.5. Boundary Conditions

Each joint of the homogeneous shell element corresponds to six degrees of freedom: three translational along local axes 1, 2, and 3; and 3 rotational about local axes 1, 2, and 3. In order to achieve compatibility with the theoretical assumptions, the translation along local axes 1 and 3, as well as the rotation around local axis 2 is unrestrained. More specifically, according to the first load case which corresponds to the application of edge force, H_o , the base nodes are free to translate along local axes 1 and 3 and to rotate around local axis 2. The same also issues to the second load case, which corresponds to the application of the edge moment, M_o , around local axis 2.

3.1.6. Results' Interpretation

Figure 9 depicts the deformation of a typical shell element that belongs to the perimeter/base of the truncated spherical dome under the application of horizontal edge force, H_o and edge moment, M_o . Under both types of loading, the base points translate along local axes 1 and 3 and rotate about local axis 2.

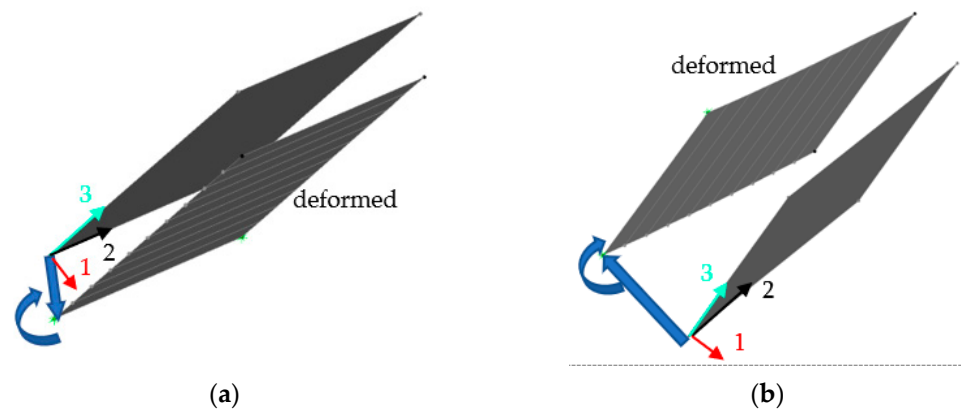


Figure 9. Deformation of typical base shell element: (a) horizontal edge force, H_o ; (b) edge moment, M_o .

The terms Δ_{φ, H_o} and Δ_{φ, M_o} correspond to the rotational displacement caused by the horizontal edge force, H_o , and edge moment, M_o , respectively. Therefore, in the framework of the finite element method, the aforementioned rotational displacements correspond to the rotation of the base joints around local axis 2, according to the loading definition. Furthermore, the terms Δ_{H, H_o} and Δ_{H, M_o} correspond to the horizontal displacement caused by the horizontal edge force, H_o , and edge moment, M_o , respectively. Hence, the translational joint displacements along local axes 1 and 3 must be analyzed along global coordinate axes X and Z, in order to determine the horizontal displacement (Figure 10).

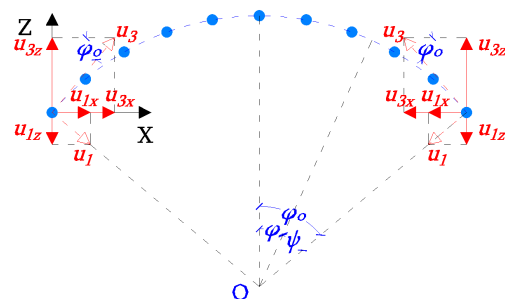


Figure 10. Determination of horizontal displacement, $\Delta_{H,i}$, based on finite element results.

The theoretical term is expressed by Equation (15).

$$\Delta_{H,i} = u_{1x} + u_{3x} = u_1 \cdot \sin\varphi_o + u_3 \cdot \cos\varphi_o \tag{15}$$

3.2. Comparison between Analytical and Numerical Results

Figure 11 depicts the typical deformation of a cross-section of the truncated spherical dome under the action of both types of loading. The grey dots represent the initial position of the finite element nodes, while the black dots represent the final deformed shape, after the application of loading. The horizontal edge force, H_o , affects the deformed shape of the spherical dome in total, while in the case of the edge moment, M_o , the deformation is more locally pronounced near the edge. Due to the symmetry of the loading and the structural geometry, as well, the results of the numerical analyses, either in terms of stresses or displacements, at any cross-section in the r-Z plane, are the same. Therefore, only the base displacements of the point which belongs to $X = -r$, $Z = 0$, and $\psi = \varphi_o$ are extruded from the results' data base.

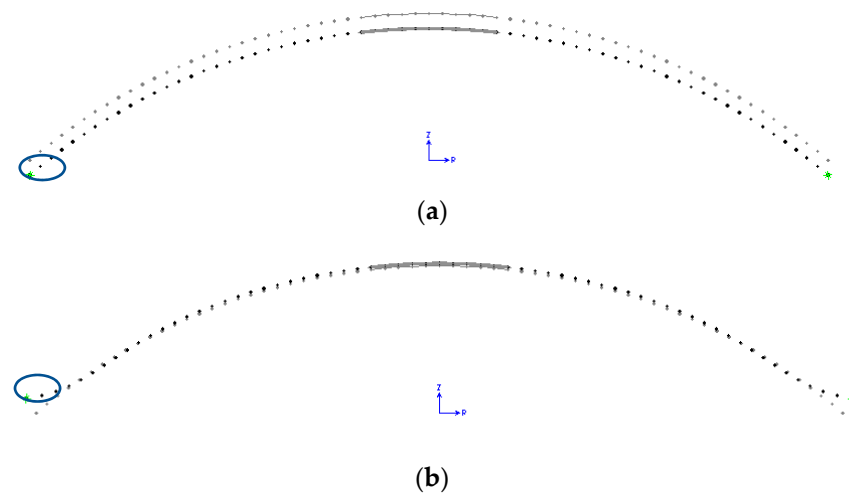


Figure 11. Typical deformation of a cross-section (grey:initial state; black: final state): (a) horizontal force, H_o ; (b) moment, M_o ; and selected joint under consideration.

Figures 12–15 depict the comparison diagrams between the results of the theoretical and numerical analyses for the four ratios of r/t . In particular, the blue dashed line corresponds to the analytical results according to the first approach (Equation (10)), while the blue continuous line corresponds to the analytical results according to the second approach (Equation (13)). Moreover, the red dashed line corresponds to the numerical results under the assumption of a coarse mesh discretization, while the continuous one is under the assumption of a dense mesh discretization. Each black dashed line depicted in the XY plane of the 3D diagrams corresponds to the radius of the spherical cap from a roll-down angle from 5° to 90° .

Figure 12 depicts the results of a very thin shell, which is characterized by $r/t = 1000$. The two analytical approaches coincide, except in the case of the rotational displacement due to edge moment loading, Δ_{φ, M_o} , and for small values of roll-down angles. The aforementioned difference is attributed to the dependence of the rotation on trigonometric terms of the roll-down angle, according to the second theoretical approach. The existence of the trigonometric term k_1 (Equation (13a)), in the denominator of Δ_{φ, M_o} (Equation (13f)), alters the analytical results for small values of φ_o . Furthermore, the difference between the coarse and dense finite element formulation is obvious for large numbers of roll-down angles for all degrees of freedom and under both loading cases. On the contrary, for small values of roll-down angles, the coarse discretization scheme suffices and converges to the second theoretical approach. The aforementioned can be explained by the fact that at small values of φ_o , the radius of the spherical cap, r_o and consequently, the perimeter of the spherical cap, L_o , receives small values. Therefore, taking into account the small thickness, t , the selection of the discretization at 1° or 2° angles is meaningless.

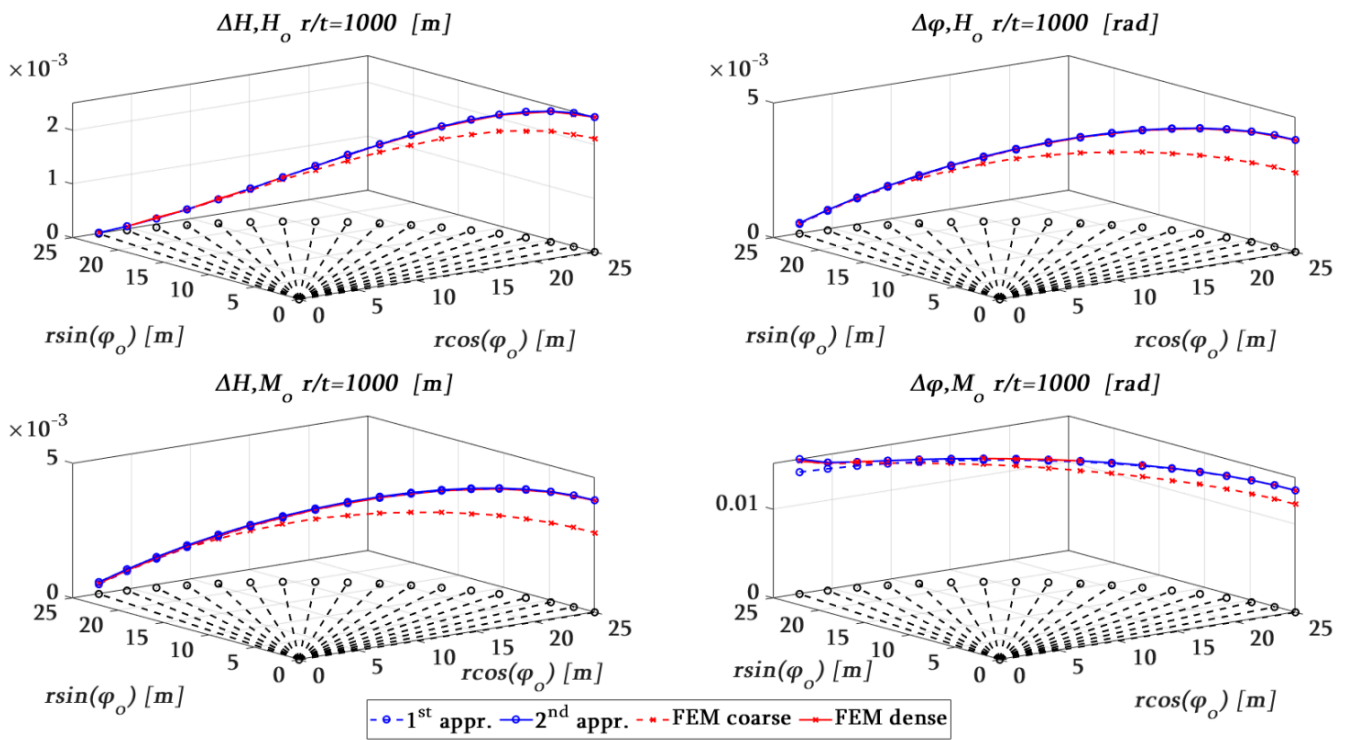


Figure 12. Dome's base displacements for $r/t = 1000$.

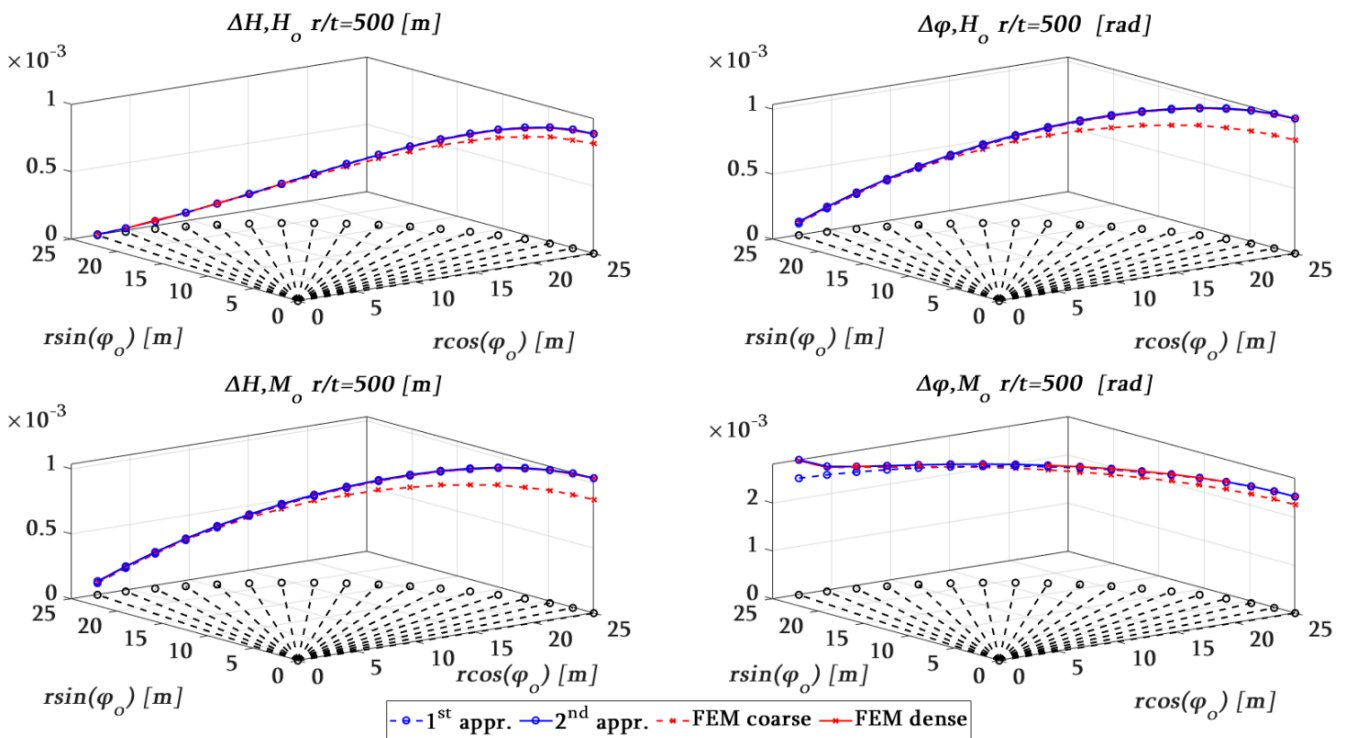


Figure 13. Dome's base displacements for $r/t = 500$.

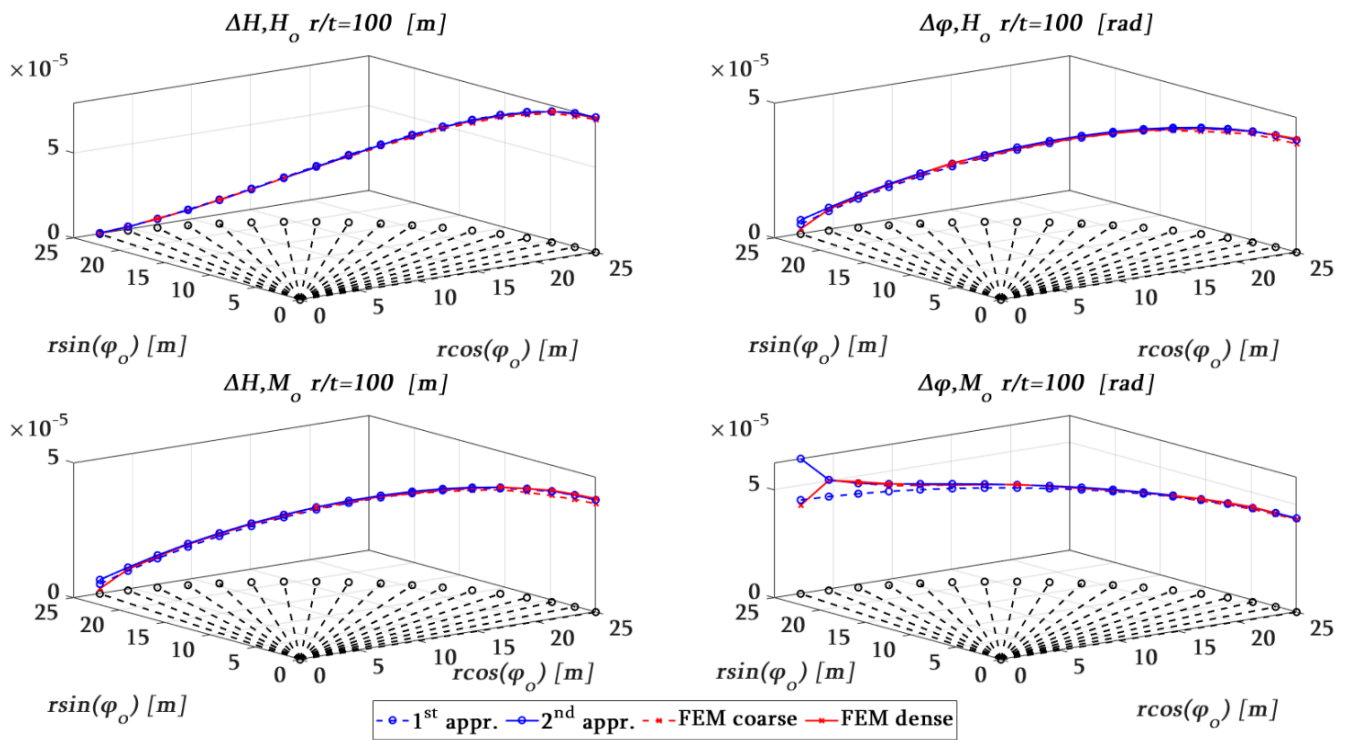


Figure 14. Dome's base displacements for $r/t = 100$.

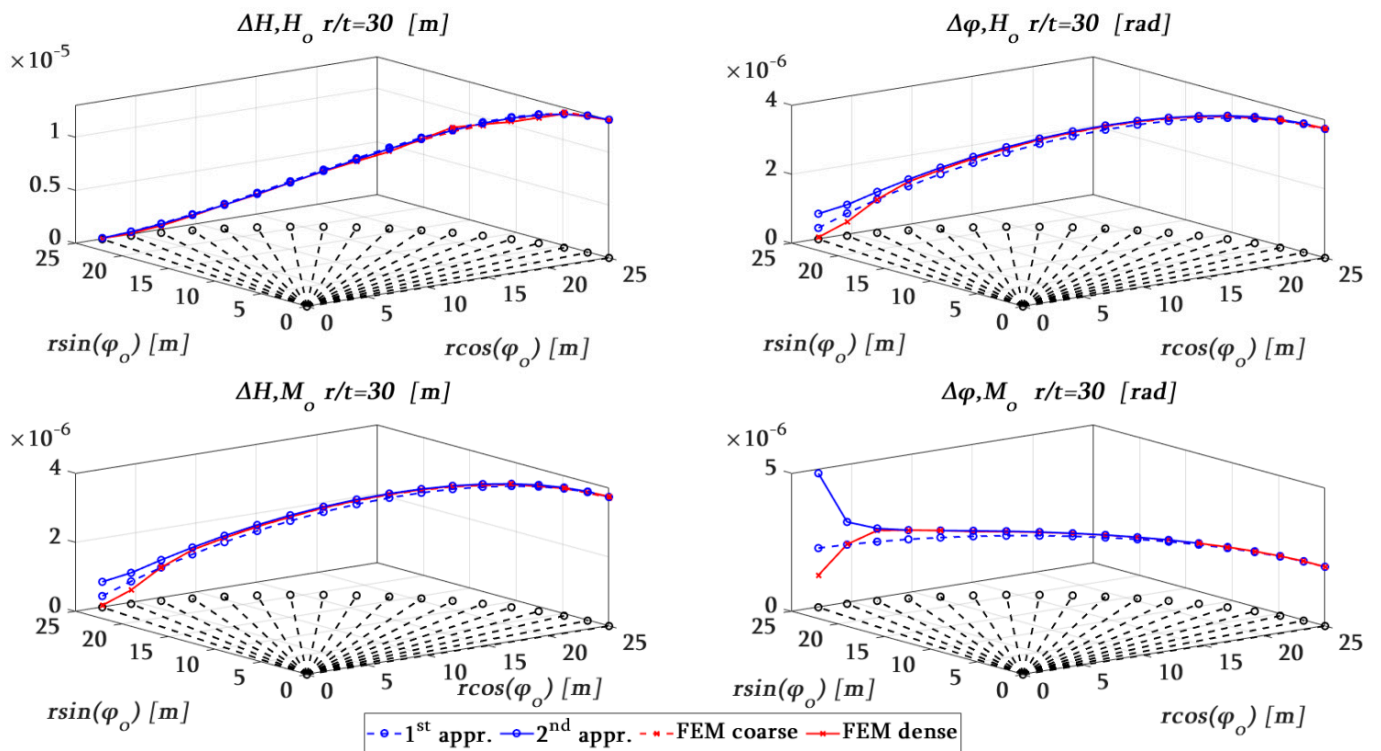


Figure 15. Dome's base displacements for $r/t = 30$.

Therefore, in the case of very thin shells characterized by $r/t = 1000$, the following two cases can be distinguished: (i) large values of roll-down angles, $\varphi_o \geq 20^\circ$, at which a dense mesh discretization scheme must be applied; (ii) small values of roll-down angles, $\varphi_o < 20^\circ$, at which a coarse mesh discretization scheme suffices.

Figure 13 depicts the results of a very thin shell, which is characterized by $r/t = 500$. Both translational and rotational displacements receive smaller values than the case of $r/t = 1000$. The results of the two analytical approaches coincide, except in the range of small values of roll-down angles ($\varphi_o < 20^\circ$) for rotational displacements under the application of edge moments, $\Delta_{\varphi,Mo}$. The discrepancy between the results of a coarse and a dense finite element discretization mesh are prominent for large values of roll-down angles ($\varphi_o \geq 30^\circ$), for all the degrees of freedom. The dense finite element mesh provides the best coincidence with the results of the second theoretical approach. However, it has to be pointed out that the coarse finite element mesh also produces excellent results for $\Delta_{\varphi,Mo}$ in the range of small values of roll-down angles.

Therefore, in the case of very thin shells characterized by $r/t = 500$, the following two cases can be distinguished: (i) large values of roll-down angles, $\varphi_o \geq 30^\circ$, at which a dense mesh discretization scheme must be applied; (ii) small values of roll-down angles, $\varphi_o < 30^\circ$, at which a coarse mesh discretization scheme suffices.

Figure 14 depicts the results of a thin shell, which is characterized by $r/t = 100$. All four approaches are in excellent coincidence, except for the case of the smallest roll-down angle, which equals 5° . Furthermore, the difference between the two theoretical approaches regarding the term $\Delta_{\varphi,Mo}$ for small values of roll-down angles ($\varphi_o < 40^\circ$) remains characteristic. Therefore, in the case of thin shells characterized by $r/t = 100$, the finite element density discretization does not affect the results except in the case of $\varphi_o = 5^\circ$.

Figure 15 depicts the results of a thin shell, which is characterized by $r/t = 30$ and belongs to the transitional area of the definition between “thin” and “thick” shells. The difference between the first and second theoretical approach is not only detected in $\Delta_{\varphi,Mo}$ terms but also in $\Delta_{\varphi,Ho}$, which is equal to $\Delta_{H,Mo}$ in the range of roll-down angles less than 50° . Another interesting observation refers to the coincidence of the results between the coarse and dense finite element discretization. The aforementioned can be explained by the following. Taking into account that the dome’s thickness receives a large value ($t = r/30 = 0.833$ m), even the coarse mesh, which corresponds to an angle of 2° , can be considered as a dense one, which corresponds to an angle of 1° . Furthermore, for all degrees of freedom, except the translational one, $\Delta_{H,Ho}$, a great discrepancy can be noticed between the second theoretical approach and the finite element results in the small range of roll-down angles, $\varphi_o \leq 10^\circ$. The aforementioned is attributed to the fact that the dome can be considered as a “thick” shell but also as a “shallow” one as well.

Therefore, according to Figure 15, in the case of shells characterized by $r/t = 30$, the finite element density discretization does not affect the results. Furthermore, the discrepancy between the two theoretical approaches cannot be ignored for values of roll-down angles that are smaller than 50° .

The previous comparison of the results was performed optically. Since data already exist, the comparison can be also performed statistically. Therefore, in order to quantify the error according to the second (2nd) analytical approach, the Mean Average Error is implemented, which is described by Equation (16).

$$MPE = \frac{100\%}{n} \cdot \sum_{i=1}^n \frac{a_i - f_i}{a_i} \quad (16)$$

where n is the number of samples and is equal to 18; a_i is the value of displacements for each degree of freedom according to the second analytical approach; and f_i is the corresponding value of displacements according to the three remaining approaches, which are regarding the first (1st) analytical approach, the coarse mesh finite element formulation, and the dense mesh finite element formulation. Table 2 presents the calculated Mean Average Errors for each one of the aforementioned cases.

Table 2. Mean Average Error quantification according to the 2nd analytical approach in [%].

r/t	1st Analytical				FEM Coarse				FEM Dense			
	Δ_{H,H_0}	Δ_{φ,H_0}	Δ_{H,M_0}	Δ_{φ,M_0}	Δ_{φ,H_0}	Δ_{φ,H_0}	Δ_{H,M_0}	Δ_{φ,M_0}	Δ_{H,H_0}	Δ_{φ,H_0}	Δ_{H,M_0}	Δ_{φ,M_0}
1000	−0.67	3.2	1.74	8.13	17.67	6.70	−0.14	2.24	0.15			
500	−0.97	2.44	2.41	4.28	9.21	3.92	−0.01	0.90	0.09			
100	−1.84	5.44	5.44	3.29	6.43	2.84	2.70	4.99	2.05			
30	−1.74	9.93	9.94	6.08	10.56	6.26	6.26	10.15	6.02			

The following observations can be made: (i) the increase in the ratio r/t results to an increase in the Mean Average Error for all the degrees of freedom and for all of the approaches; (ii) the Mean Average Error is the same for all the approaches in the cases of the coupling terms, Δ_{φ,H_0} and Δ_{H,M_0} , since their values are the same for each roll-down angle, φ_0 ; (iii) the higher values of Mean Average Errors correspond to the coarse mesh finite element formulation except for ratios r/t equal to 100 and 30, at which the first analytical approach deviates from the solution of the second analytical approach for the Δ_{φ,M_0} degree of freedom; (iv) the smallest values of Mean Average Errors correspond to the dense mesh finite element formulation; (v) for the ratio r/t equal to 30, the coarse and dense finite element formulation produce results of the same quality.

4. Conclusions

The present paper refers to the in-depth verification of the application of the finite element method in order to determine the base displacements of a thin spherical dome, which is truncated for various roll-down angles under the action of edge horizontal forces and rotational moments. Some of the general basic conclusions are summarized in the following.

- The validation and verification of finite element models implemented to study a specific engineering case are not only crucial but also of vast importance.
- In the absence of laboratory or in situ experiments, the engineer should refer to the results of an analytical approach. The verified finite element model, even under the assumptions of linearity and elasticity, forms a stable basis for its evolution and development under non-linear assumptions.
- Special attention should be given by the engineer on the assumptions by which an analytical approach is governed and on the appropriate available finite element tools.
- The engineer must be fully conversant with the capabilities or restrictions of the available finite element software.

Furthermore, some of the conclusions derived by the specific problem under study are the following:

- Two theoretical and analytical approaches have been implemented. The basic difference refers to the dependency of the rotational displacements caused by edge moments, on the value of the roll-down angle for all the considered values of the ratio, r/t .
- As the ratio, r/t , becomes larger, or in other words, the shell becomes thicker, the discrepancy between the two analytical approaches is evident not only in rotational but also in translational displacements.
- The numerical results considering the dense finite element discretization approach are in excellent agreement with the analytical ones derived by the second analytical approach for all ratios of r/t .
- The effect of the finite element mesh discretization on numerical results is more pronounced in the case of very thin shells. In particular, for $r/t \leq 500$ and for the roll-down angle $\varphi_0 \geq 30^\circ$, a dense mesh should be applied. On the contrary, as the shell thickness increases ($r/t \geq 100$), no difference between the coarse and dense mesh is detected.

- Differences between the numerical and analytical results are detected for the case of $r/t = 30$, which belongs to the transitional area of definition between “thin” and “thick” shells but only in the range of small values of roll-down angles ($\varphi_0 \leq 10^\circ$). The behavior of the dome as a “thick shallow” shell cannot be captured by the implementation of homogeneous and thin shell elements. The use of the thick shell formulation or of three-dimensional finite elements is proposed.
- According to the aforementioned conclusions, the main future research direction regards the finite element modeling of “thick shallow” shells by the use of three-dimensional elements.

In conclusion, the process of verification of the numerical models demands a thorough knowledge not only of the available software and its capabilities, but also on the physics of the case study, which can be derived by analytical solutions. Although, in most cases, the theoretical approach is usually based on assumptions that simplify the case study, a successful verification will form the basis for the development of more sophisticated numerical models.

Author Contributions: Conceptualization, V.G.T.; methodology, V.G.T.; software, V.G.T.; validation, V.G.T.; formal analysis, V.G.T.; investigation, V.G.T.; resources, V.G.T. and T.K.M.; data curation, V.G.T.; writing—original draft preparation, V.G.T.; writing—review and editing, V.G.T. and T.K.M.; visualization, V.G.T.; supervision, V.G.T. All authors have read and agreed to the published version of the manuscript.

Funding: This research received no external funding.

Data Availability Statement: Data will be shared upon request.

Conflicts of Interest: The authors declare no conflict of interest.

References

1. Kwasniewski, L.; Bojanowski, C. Principles of verification and validation. *J. Struct. Fire Eng.* **2015**, *6*, 29–40. [[CrossRef](#)]
2. Roache, P. *Verification and Validation in Computational Science and Engineering*, 1st ed.; Hermosa Publishers: Albuquerque, NM, USA, 1998.
3. Niemi, H.A. Benchmark computations of stresses in a spherical dome with shell finite elements. *SIAM J. Sci. Comput.* **2016**, *38*, B440–B457. [[CrossRef](#)]
4. Pitolakis, K.; Terzi, V. Experimental and theoretical SFSI studies in a model structure in Euroseistest. In *Special Topics in Earthquake Geotechnical Engineering. Geotechnical, Geological and Earthquake Engineering*, 1st ed.; Sakr, M., Ansal, A., Eds.; Springer: Dordrecht, The Netherlands, 2012; Volume 16, pp. 175–215. [[CrossRef](#)]
5. Manolis, G.D.; Makarios, T.K.; Terzi, V.; Karetsou, I. Mode shape identification of an existing three-story flexible steel stairway as a continuous dynamic system. *Theor. Appl. Mech.* **2015**, *42*, 151–166. [[CrossRef](#)]
6. Chandrashekhra, K. *Analysis of Thin Concrete Shells*, 2nd ed.; New Age International Publishers: Bengaluru, India, 1995.
7. Sun, G.; Longman, R.W.; Betti, R.; Che, Z.; Xue, S. Observer Kalman filter identification of suspen-dome. *Math. Prob. Eng.* **2017**, *2*, 16101534. [[CrossRef](#)]
8. Hussain, N.L.; Mohammed, S.A.; Mansor, A.A. Finite element analysis of large-scale reinforced concrete shell of domes. *J. Eng. Sci. Technol.* **2020**, *15*, 782–791.
9. Kobiela, S.; Zamiar, Z. Oval concrete domes. *Arch. Civ. Mech. Eng.* **2017**, *17*, 486–501. [[CrossRef](#)]
10. Sadowski, A.J.; Rotter, J.M. Solid or shell finite elements to model thick cylindrical tubes and shells under global bending. *Int. J. Mech. Sci.* **2013**, *74*, 143–153. [[CrossRef](#)]
11. Makarios, T.K. Equivalent torsional-warping stiffness of cores with thin-walled open cross-section using the Vlasov torsion theory. *Am. J. Eng. App. Sci.* **2023**, *16*, 44–55. [[CrossRef](#)]
12. Donell, L.H. *Stability of Thin-Walled Tubes under Torsion*; NACA Report No. 479; National Advisory Committee for Aeronautics: Washington, DC, USA, 1933.
13. Timoshenko, S.P. *History of Strength of Materials*, 1st ed.; McGraw-Hill Book Company: New York, NY, USA, 1953.
14. Novozhilov, V.V. *The Theory of Thin Shells*, 2nd ed.; P. Noordhoff Ltd.: Groningen, The Netherlands, 1964.
15. Calladine, C.R. *Theory of Shell Structures*, 1st ed.; Cambridge University Press: Cambridge, UK, 1983.
16. Bushnell, D. *Computerized Buckling Analysis of Shells*, 1st ed.; Martinus Nijhoff Publishers: Morsel, Belgium, 1985.
17. Brush, D.O.; Almroth, B.O. *Buckling of Bars, Plates and Shells*; McGraw-Hill Book Company: New York, NY, USA, 1975.
18. Seide, P. *Small Elastic Deformations of Thin Shells*; P. Noordhoff Ltd.: Groningen, The Netherlands, 1975.
19. Reissner, E. The effect of transverse shear deformation on the bending of elastic plates. *J. Appl. Mech.* **1945**, *12*, A69–A77. [[CrossRef](#)]

20. Mindlin, R.D. Influence of rotary inertia and shear on flexural motions of isotropic elastic plates. *J. Appl. Mech.* **1951**, *18*, 31–38. [[CrossRef](#)]
21. Euler, L. De motu vibratorio laminarum elasticarum, ubi plures novae vibrationum species hactenus non pertractatae evoluntur. *Novi Comment. Acad. Sci. Metrop.* **1773**, *17*, 449–487.
22. Timoshenko, S.P. On the correction factor for shear of the differential equation for transverse vibrations of bars of uniform cross-section. *Lond. Edinb. Dubl. Phil. Mag.* **1921**, *41*, 744–746. [[CrossRef](#)]
23. Elishakoff, I. Who developed the so-called Timoshenko beam theory? *Math. Mech. Solids* **2020**, *25*, 97–119. [[CrossRef](#)]
24. Terzi, G.V. Soil-structure interaction effects on the flexural vibrations of a cantilever beam. *Appl. Math. Model.* **2021**, *97*, 138–181. [[CrossRef](#)]
25. Vlassov, S. *Allgemeine Schalentheorie und ihre Anwendung in der Technik*; Akademie-Verlag: Berlin, Germany, 1958.
26. Timoshenko, S.; Woinowsky-Krieger, S. *Theory of Plates and Shells*; McGraw-Hill: New York, NY, USA, 1959.
27. Flügge, W. *Statik und Dynamik der Schalen*; Springer: Berlin/Heidelberg, Germany, 1975.
28. Heyman, J. *Equilibrium of Shell Structures*; Oxford University Press: Oxford, UK, 1977.
29. Mbakogu, F.C.; Pavlović, M.N. Bending and stretching actions in shallow domes. Part 1. Analytical derivations. *Thin-Walled Struct.* **1996**, *26*, 61–82. [[CrossRef](#)]
30. Mbakogu, F.C.; Pavlović, M.N. Bending and stretching actions in shallow domes. Part 2. A comparative study of various boundary conditions. *Thin-Walled Struct.* **1996**, *26*, 147–158. [[CrossRef](#)]
31. Barsotti, R.; Stagnari, R.; Bennati, S. Searching for admissible thrust surfaces in axial-symmetric masonry domes: Some first explicit solutions. *Eng. Struct.* **2021**, *242*, 112547. [[CrossRef](#)]
32. Cusano, C.; Montanino, A.; Olivieri, C.; Paris, V.; Cennamo, C. Graphical and Analytical Quantitative Comparison in the Domes Assessment: The Case of San Francesco di Paola. *Appl. Sci.* **2021**, *11*, 3622. [[CrossRef](#)]
33. Bacigalupo, A.; Brencich, A.; Gambarotta, L. A simplified assessment of the dome and drum of the Basilica of S. Maria Assunta in Carignano in Genoa. *Eng. Struct.* **2013**, *56*, 749–765. [[CrossRef](#)]
34. Balasubramanian, M.; Sathish Kumar, M.K.; Stalin, B.; Ravichandran, M. Theoretical predictions and experimental investigation on three stage hemispherical dome in superplastic forming process. *Mater. Today Proc.* **2020**, *24*, 1424–1433. [[CrossRef](#)]
35. Cusano, C.; Angjeliu, G.; Montanino, A.; Zuccaro, G.; Cennamo, C. Considerations about the static response of masonry domes: A comparison between limit analysis and finite element method. *Int. J. Mason. Res. Innov.* **2021**, *6*, 502–528. [[CrossRef](#)]
36. Padovec, Z.; Vondráček, D.; Mareš, T. The analytical and numerical stress analysis of various domes for composite pressure vessels. *Appl. Comput. Mech.* **2022**, *16*, 151–166. [[CrossRef](#)]
37. Al-Hashimi, H.; Seibi, A.C.; Molki, A. Experimental Study and Numerical Simulation of Domes under Wind Load. In Proceedings of the ASME 2009 Pressure Vessels and Piping Division Conference, Prague, Czech Republic, 26–30 July 2009; pp. 519–528.
38. Hamed, E.; Bradford, M.A.; Gilbert, R.I.; Chang, Z.-T. Analytical Model and Experimental Study of Failure Behavior of Thin-Walled Shallow Concrete Domes. *J. Struct. Eng.* **2011**, *137*, 88–99. [[CrossRef](#)]
39. Shaheen, Y.B.I.; Eltaly, B.A.; Haneesh, A.A. Experimental and FE simulations of ferrocement domes reinforced with composite materials. *Concr. Res. Lett.* **2014**, *5*, 873–887.
40. Gohari, S.; Sharifi, S.; Burvill, C.; Mouloudi, S.; Izadifar, M.; Thissen, P. Localized failure analysis of internally pressurized laminated ellipsoidal woven GFRP composite domes: Analytical, numerical, and experimental studies. *Arch. Civ. Mech. Eng.* **2019**, *19*, 1235–1250. [[CrossRef](#)]
41. Zona, R.; Ferla, P.; Minutolo, V. Limit analysis of conical and parabolic domes based on semi-analytical solution. *J. Build. Eng.* **2021**, *44*, 103271. [[CrossRef](#)]
42. Nodargi, N.A.; Bisegna, P. Minimum thrust and minimum thickness of spherical masonry domes: A semi-analytical approach. *Eur. J. Mech. A/Solids* **2021**, *87*, 104222. [[CrossRef](#)]
43. Zona, R.; Esposito, L.; Palladino, S.; Totaro, E.; Minutolo, V. Semianalytical Lower-Bound Limit Analysis of Domes and Vaults. *Appl. Sci.* **2022**, *12*, 9155. [[CrossRef](#)]
44. Girkman, K. Die Faltwerke. In *Flächentragwerke*; Springer: Vienna, Austria, 1963. [[CrossRef](#)]
45. Pitkäranta, J.; Babuška, I.; Szabó, B. The Girkman problem. *IACM Expr.* **2008**, *22*, 28.
46. Szabó, B.; Babuška, I.; Pitkäranta, J.; Nervi, S. The problem of verification with reference to the Girkman problem. *Eng. Comput.* **2010**, *26*, 171–183. [[CrossRef](#)]
47. Niemi, A.H.; Babuška, I.; Pitkäranta, J.; Demkowicz, L. Finite element analysis of the Girkman problem using the modern hp-version and the classical h-version. *Eng. Comput.* **2012**, *28*, 123–134. [[CrossRef](#)]
48. Pitkäranta, J.; Babuška, I.; Szabó, B. The dome and the ring: Verification of an old mathematical model for the design of a stiffened shell roof. *Comput. Math. Appl.* **2012**, *64*, 48–72. [[CrossRef](#)]
49. Novozhilov, V.V. *Thin Shell Theory*; Wolter-Noordhoff: Groningen, The Netherlands, 1970.
50. Gould, P.L. *Analysis of Shells and Plates*; Springer: New York, NY, USA, 1988.
51. Zingoni, A. *Shell Structures in Civil and Mechanical Engineering: Theory and Closed-Form Analytical Solutions*; Thomas Telford, The Institution of Civil Engineers: London, UK, 1997.
52. Zingoni, A.; Enoma, N. On the strength and stability of elliptic toroidal domes. *Eng. Struct.* **2020**, *207*, 110241. [[CrossRef](#)]
53. Geckeler, J. Über die Festigkeit achsensymmetrischer Schalen. *Forschungsergebnisse Auf Dem Geb. Dse Ingenieurwesens* **1926**, *276*, 52.
54. Hetényi, M. Spherical shells subjected to axial symmetrical bending. *Publ. Int. Assoc. Brid. Struct. Eng.* **1938**, *5*, 173.

-
55. *SAP2000v.24*; Computers and Structures, Inc.: Berkeley, CA, USA, 2022.
 56. Taylor, R.L.; Simo, J.C. Bending and membrane elements for analysis of thick and thin shells. In Proceedings of the NUMETA, Swansea, Wales, 7–11 January 1985.
 57. Ibrahimbegovic, A.; Wilson, E.L. A unified formulation for triangular and quadrilateral flat shell finite elements with six nodal degrees of freedom. *Commun. Appl. Numer. Methods* **1991**, *7*, 1–9. [[CrossRef](#)]

Disclaimer/Publisher’s Note: The statements, opinions and data contained in all publications are solely those of the individual author(s) and contributor(s) and not of MDPI and/or the editor(s). MDPI and/or the editor(s) disclaim responsibility for any injury to people or property resulting from any ideas, methods, instructions or products referred to in the content.